Mega Satellite Constellation System Optimization: From a Network Control Structure Perspective

Sijing Ji, Di Zhou, *Member, IEEE*, Min Sheng, *Senior Member, IEEE*, and Jiandong Li, *Fellow, IEEE*

***Abstract*— The network control plays a vital role in the mega satellite constellation (MSC) to coordinate massive network nodes to ensure the effectiveness and reliability of operations and services for future space wireless communications networks. One of the critical issues in satellite network control is how to design an optimal network control structure (ONCS) by configuring the least number of controllers to achieve efficient control interaction within a limited number of hops. Considering the wide coverage, rising capacity, and no geographical constraints of space platforms, this paper contributes to designing the ONCS by constructing an optimal space control network (SCN) to improve the temporal effectiveness of network control. Specifically, we formulate the optimal SCN construction problem from the perspective of satellite coverage factors, and apply geometric topology analysis to derive both the conditions for constructing the optimal SCN and the formulaic conclusions for SCN and MSC configurations (i.e., scale and structure). From numerical results, we investigate the tradeoff between network scale, the number of controllers, and control delays in several satellite network control scenarios, to provide guidelines for the MSC control. We also design the optimal SCN for an existing MSC system to demonstrate the effectiveness of the proposed ONCS.**

***Index Terms*— Future space wireless communications networks, mega satellite constellation, satellite network control structure, space control networks.**

I. Introduction

RECENTLY, the idea of constructing Space Internet [1], [2] and Internet of Space Things [3], [4] as well as the vision of integrating satellite networks into future 6G systems [5]–[7] have once again stimulated the research upsurge of satellite networks in future wireless communications networks [8]. However, different from the network configurations (i.e., scale and structure) decades ago [9], the emerging low Earth orbit (LEO) satellite constellations, such as StarLink and OneWeb, have gradually become dense and large-scale to improve network coverage and capacity for worldwide broadband provision [2]. Eventually, the LEO satellite constellation will be expanded to form a mega satellite constellation (MSC) containing at least 10,000 space platforms [1]. To cope with the rapid growth in the LEO constellation scale, numerous researchers have rethought some key system issues [8], such as constellation design [4], [10], routing [11], mobility management [12], strategies for integrated terrestrial-satellite offloading [13], and analysis of satellite uplinks [14] and downlinks [15]. However, the realization of these technologies is inseparable from the support of efficient network control techniques. Therefore, this paper concentrates on network control for the MSC.

Network control plays a pivotal role in satellite networks, such as instruction distributing for earth observation [16], network management for mobility [12] and resources [17], and fault monitoring and maintenance, to ensure the effectiveness and reliability of network operations and services. However, network controllers are required to coordinate a large number of network nodes, process vast amounts of control signaling, and quickly respond to services and failures in the MSC, which are not considered in the previous systems. Therefore, how to design an optimal network control structure (ONCS) by configuring the least number of controllers to achieve efficient control interaction within a limited number of hops is a critical issue in MSC.

Current satellite network control structures majorly include ground-based and space-based mechanisms. The ground-based network control deploys the controllers on the ground stations (GSs) located at pre-selected geographic locations [18]. However, this mechanism has inherent deficiencies that global GS deployments could not be realized in reality due to political and geographic factors [19], [20]. Thus, some control signaling needs to forward to the nearest GS by inter-satellite links (ISLs) to complete control procedures with potentially high latency. In MSC, a large amount of signaling backhaul will result in severe local network congestion around GS and aggravate network control load and overheads, which further worsen the control delays.

In order to solve the problems caused by the inability to deploy GSs globally and the growth of constellation scale, satellites can be equipped with controller payload, such as software-defined networking (SDN) controller [19]–[24], generation NodeB (gNB) [12], [25], and other payloads with controller abilities [26], [27], to implement space-based network control for satellites, users, and services. At present, two

Manuscript received November 10, 2020; revised May 15, 2021; accepted July 13, 2021. Date of publication August 3, 2021; date of current version February 14, 2022. This work was supported in part by the Natural Science Foundation of China under Grant U19B2025, Grant 61725103, and Grant 62001347; in part by the China Postdoctoral Science Foundation under Grant 2019TQ0241 and Grant 2020M673344; and in part by the Fundamental Research Funds for the Central Universities under Grant XJS200117. The associate editor coordinating the review of this article and approving it for publication was G. C. Alexandropoulos. *(Corresponding author: Di Zhou.)*

The authors are with the State Key Laboratory of Integrated Services Networks, Xidian University, Xi'an 710071, China (e-mail: sjji@stu.xidian.edu.cn; zhoudi@xidian.edu.cn; msheng@mail.xidian.edu.cn; jdli@mail.xidian.edu.cn).

Color versions of one or more figures in this article are available at https://doi.org/10.1109/TWC.2021.3100247.

Digital Object Identifier 10.1109/TWC.2021.3100247

schemes are state of the art in the design of space-based network control structure: controller placement and control network construction. On the one hand, the controller placement is to deploy controllers on some existing space platforms [24]. This network control structure does not realize the physical separation of data and control plane. Moreover, the controllers need to interact constantly to collect information of the entire network [28], so the control load may be very heavy that occupies the resources for data transmission. Besides, the controller quantity has great relation to the network scale. On the other hand, the geosynchronous orbit (GSO) and medium Earth orbit (MEO) satellites (i.e., non-LEO satellite) have been widely recognized by academia as control nodes to implement network control for LEO satellites with theoretical support in [12], [19]–[23], and [27]. In industry, some commercial non-LEO satellites have already equipped with regenerative payloads with software-defined radio (SDR) (e.g., MicroGEO [29]) and software-defined satellite (SDS) (e.g., Boeing's 702X family, OneSat, and O3b mPOWER [30]) technologies for not only data/signal processing but also flexibility, reconfigurability, and lower cost of satellites, which provides technological feasibility of implementing the space control network. Benefiting from the wide coverage, no geographical restrictions, longer lifetime, and rising capabilities of non-LEO satellites [19], [27], constructing a control network on the non-LEO satellite layer can effectively reduce controller quantities, achieve global efficient network control, and realize the physical and logical separation of data and control plane, which may be the best option for the MSC control.

In this paper, we design the ONCS by constructing the optimal space control network (SCN) on non-LEO satellites for LEO mega satellite constellations. With the geometric formulation of the problem, both the optimal conditions and the formulaic conclusions are derived to guide the design of network configurations for MSC and SCN.

The main contributions of this paper are summarized as the following triples:

- Considering that the impact of satellite beam shape and size on the satellite coverage further affects the inter-layer network configurations, we investigate and formulate the practical coverage models of the non-LEO satellite to LEO satellites into the optimal SCN construction problem. On this basis, given the coverage features and the controllable hops of non-LEO satellite controllers, the conditions for constructing the optimal SCN can be quickly determined by a series of discriminants. More importantly, the corresponding network configurations of both LEO and non-LEO satellite layers can also be derived by formulaic conclusions rapidly.
- Any optimal network configuration can be expanded into a larger-scale satellite network geometrically, such as an MSC. Notably, our work caters to the development trends of the future mega satellite constellation, while the computational complexity of the methodology will not change as the network scale increases.
- Through numerical results, we obtain the following two interesting findings: (1) blindly improving the controllable hops cannot facilitate the rapid and continuous decline of the number of controllers; (2) there exists a tradeoff between the number of controllers and control delays. In practice, by designing appropriate controllable hops, orbital altitudes, and satellite coverage angles according to delay demands and network scale, the performance between the number of controllers and control delays can strike a balance. Furthermore, we also design the optimal SCN for an existing MSC system (i.e., OneWeb) to demonstrate the effectiveness of the proposed ONCS.

The remainder of this paper is organized as follows. The subsequent section reviews the related work in literature. Then, the models for networks and typical satellite coverage are defined and illustrated in Section III. Next, we propose and prove the lemmas and theorems for optimal SCN construction in Section IV. Then, results for common network control scenarios and the optimal SCN of OneWeb are shown and discussed in Section V. Finally, we summarize our work.

II. Related Work

Concerning the network control structure design, most recent literature has concentrated on SDN controller placement in satellite networks [20], [24] as well as satellite-terrestrial integrated networks [31], [32]. The main differences among these existing controller placement strategies are optimal metrics and problem solutions.

The optimal metrics can be considered in many aspects [33], in which optimal performance [24], best resilience [20], maximum reliability [31], [32], and minimum cost [20] are the most common single metrics in satellite-related networks. Some work formulates multiple metrics as the objectives to make a more integrated optimization on controller placement [20].

In satellite-related networks, most controller placement problems are modeled as undirected graphs and formulated into optimization. To solve these NP-hard problems, authors in [24] developed the problem into an integer linear programming that can be calculated by linear solvers (e.g., Gurobi). Still, this method usually requires partial reformulation to adapt to the optimizer. Then, some work proposed heuristic algorithms based on simulated annealing to obtain a near-optimal solution [20], [31]. Further, to get a better near-optimal solution with shorter running time, authors in [32] proposed a metaheuristic approach that applied the simulated annealing procedure twice and genetic algorithm.

However, the computational complexity of optimization makes it almost impossible to efficiently apply in MSC scenarios, which none of these work has considered, unfortunately. Noteworthily, some existing efforts committed to deriving closed-form formulae with lower complexity, which can be borrowed from our scenarios. Specifically, by virtue of principles of error correction code under Lee distance, Bae *et al.* gave out a series of theorems that enable the optimal resource placement in the torus-based networks rapidly [34]. Krishnan *et al.* presented closed-form formulae for some special cases in cache location problems [35].

Concerning the satellite constellation design, existing studies mainly focus on the Earth observation satellite (EOS) constellation and the LEO satellite constellation. Early EOS

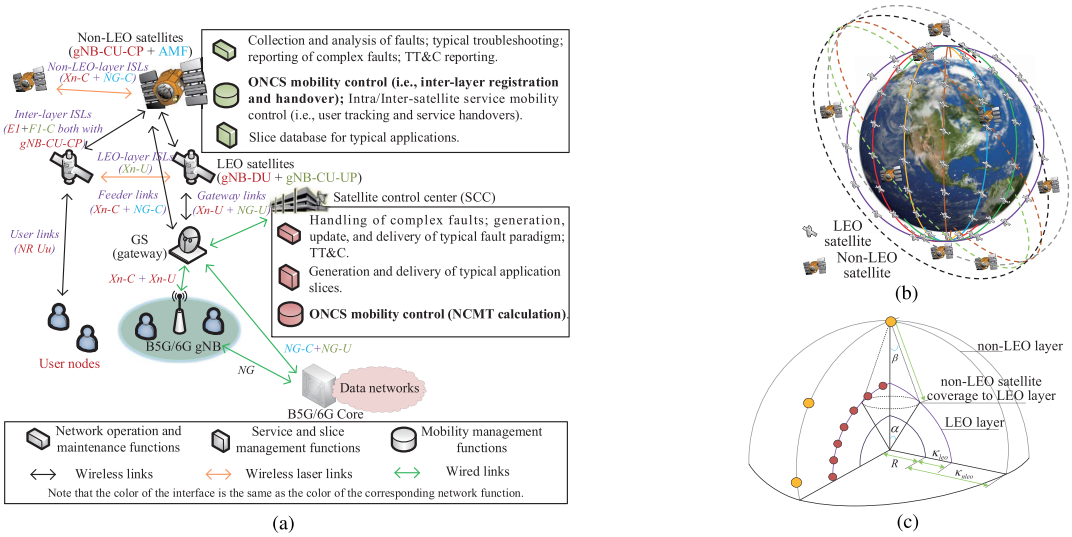

Fig. 1. System models: a) a double-layer satellite network architecture integrated with B5G/6G; b) an example of a double-layer satellite network with 8 (i.e., 4×2) non-LEO satellites and 96 (i.e., 6×16) LEO satellites, in which each non-LEO satellite controller controls 12 LEO satellites; c) geometric illustration of non-LEO satellite coverage to LEO satellites.

constellation design generally relies on commercial tools (e.g., Satellite Tool Kit (STK)) [36]. Recently, evolutionary algorithms have been widely used in the optimal design of EOS constellation to meet the expected metrics [37]. However, due to the low demand for the number of EOSs, even the design of a heterogeneous and multi-layer EOS constellation does not exceed 100 satellites [37]. To avoid much reliance on commercial tools and design larger-scale satellite constellations, researchers presented a modular and highly customizable large-scale constellation design framework to design robust constellation for Internet of Space Things/CubeSats considering network density, coverage, and connection parameters in [4], while authors in [10] proposed a three-dimensional constellation optimization algorithm to minimize the number of LEO satellites under a polar-orbital constellation based on the derived average total backhaul capacity of terrestrial-satellite terminals. The above studies are special for constellation design. At the same time, some work advised on selecting design parameters for MSC, such as altitude, the number of satellites, and orbital inclination, by analyzing network performance metrics [15].

Although the above literature has solved many network control and constellation design problems, none of them has considered designing the ONCS by constructing an optimal SCN on the non-LEO satellite layer, nor has any literature investigated the impact of actual satellite coverage on the optimal SCN construction and given closed-form solutions for the joint design of double-layer satellite networks. Besides, most of the solutions on optimization are hard to rapidly apply to actual engineering design due to high complexity, and the results of these work also have not really reached the MSC magnitude, which are all our focuses in this paper.

III. System Models

In this section, we give network models and satellite coverage models to design the ONCS by constructing an optimal SCN on the non-LEO satellite layer.

A. Network Models

This paper considers a double-layer satellite network including a LEO satellite layer for services, a non-LEO satellite layer for assisted satellite network control, and a satellite control center (SCC) for dominated satellite network control, as shown in Fig. 1(a) and 1(b).

1) Network Architectures: The specific network nodes, interface protocols, and network functions are illustrated in Fig. 1(a) [12], where the satellite networks are integrated with terrestrial B5G/6G systems by the functions and interfaces that have been defined by 3GPP non-terrestrial networks [25] and standards [38], [39]. In detail, the LEO satellites inherit functions of gNB distributed unit (gNB-DU) and gNB central unit user plane (gNB-CU-UP) mainly for data communications and collection. The non-LEO satellites inherit the functions of the relocated access and mobility management function (AMF) and the gNB-CU control plane (gNB-CU-CP) that hosts the radio resource control (RRC) [12]. With the architectures demonstrated in Fig. 1(a), a unified network management paradigm is revealed that the non-LEO satellites should interact with the SCC to complete the satellite network control for network operation and maintenance, service and slice management, and mobility management collaboratively.

2) LEO Satellites: The set of LEO satellites with the orbital altitude of κ_{leo} kilometers (km) is denoted by $\mathcal{S}_{leo}$, where each satellite is represented as a unique identifier. The ISLs between satellites in the same or adjacent orbital plane are created by laser transceivers that have been applied in some existing satellite systems (e.g., StarLink [40] and LeoSat [41]), where the intra/adjacent-orbital plane laser ISLs (LISLs) are generally permanent even within/near the Polar regions [42], [43].[1] Since the satellite network established

[1]For some special cases that the ISL transceiver has failures or LISL between adjacent plane has temporary interruption due to the drastical variation of relative position at Poles, the system allows the control of the corresponding LEO satellites through other intra/inter-layer paths or interchangeable transceivers by failure management to ensure the reliable network control [44].

by permanent LISLs provides a good mesh network [42], we model the single LEO layer as an $N \times M$ torus lattice network with N satellite orbits and M satellites per orbit [45]. To simplify the illustration, we use lattice diagrams to represent the two-dimensional (2D) torus in this paper, and the wraparound edges exist but are not shown.

3) Non-LEO Satellites: The non-LEO satellite with the orbital altitude of κ_{nleo} km controls the LEO satellites by the equipped controller and inter-layer ISLs. Suppose that the number of non-LEO satellites in the controller set $\mathcal{Q}$ is $Q = |\mathcal{Q}|$, where $|\cdot|$ denotes the number of elements in the set. For each controller $q \in \mathcal{Q}$, the identifier vector and set of all LEO satellites it can control at time t are denoted by $\boldsymbol{c}_q(t)$ and $\mathcal{C}_q(t)$, termed a control domain (CD), which is obtained by the network control mapping (NCM) (i.e., bijection $f_t(\cdot) : q \mapsto \boldsymbol{c}_q(t)$) calculated by SCC in advance. Considering the balance of satellite storage and processing load as well as signaling overheads, controllers are expected to control the same number of LEO satellites $V = |\mathcal{C}_q(t)|$ to ensure the balanced resource usage. To cope with the mobility of non-LEO and LEO satellites, we further introduce registration and handover schemes into the models.

a) Registration: As the distance between satellites decreases in high latitudes, the number of reachable LEO satellites within J hops of a controller will increase and be redundancy. To ensure the stability of the controller load and control structure, the LEO satellites should register to the non-LEO satellite controller at the initial time or after handovers. The registration process strictly follows the mapping relations in NCM for non-repetitive control, which also weakens the physical unreality of the torus lattice models. To avoid wasting beam resources, the non-LEO satellites could scale down the coverage at high latitudes through flexible phased-array technologies to save energy.

b) Handover: Since LISLs are intermittent and cannot last for a long duration [46], the non-LEO satellites are equipped with electronically steerable radio beams to stare at the fixed controlled LEO satellites (i.e., CD) continuously to ensure a topologically stable network control structure during the period from registration to the next handover, similar to the earth-fixed footprints [47], so-called CD-fixed coverage. With a steerable beam approach that have been used in O3b MEO system [48], the ONCS handovers are triggered when the NCM uploaded by SCC changes, that is $f_t \neq f_{t_+}$, and then each non-LEO satellite controller q will perform a synchronous handover [47] to the next CD of $f_{t_+}(q)$ at time t_+, which means all LEO satellites controlled by one controller before the handover will be completely controlled by the other controller. Thereby, the domain $\mathcal{Q}$ and codomain $\mathcal{C}(t) := \{\boldsymbol{c}_q(t) \mid \forall q\}$ of $f_t(\cdot)$ are set to be constant, and only the mapping relations are changed during the system duration, that is $\forall t,\ f_t(\cdot) : \mathcal{Q} \to \mathcal{C}$.

Now, we can define the ONCS as follows.

Definition 1 (Optimal Network Control Structure): At any time t, the optimal network control structure is to realize the non-repetitive control of all controlled nodes with the least number of controllers, and each controller controls the same number of nodes, which can be defined in mathematical form as: $\forall t,\ \bigcup_{q=1}^{Q} \mathcal{C}_q(t) = \mathcal{S}_{leo}$, $\mathcal{C}_1(t) \bigcap \mathcal{C}_2(t) \bigcap \cdots \bigcap \mathcal{C}_q(t) = \varnothing$ *and* $\forall q = 1, \ldots, Q,\ |\mathcal{C}_q(t)| = V$.

The factors that affect the design of the ONCS involve the MSC configuration, the network construction cost, the storage and processing abilities of controllers, the capacity of inter-layer ISLs, the actual occupation of orbits, and the satellite coverage, where the satellite coverage directly reflects the connections between the double layers and becomes the most important factors since almost all the other factors could be mapped to the satellite coverage modeling. For example, the limited storage and processing abilities of controllers imply the need for reduction of coverage and controllable hops of the non-LEO satellites. Thus, we mainly consider the ONCS from the perspective of the satellite coverage related to coverage shape, size, inter-layer distance $\xi = \kappa_{nleo} - \kappa_{leo}$, and controllable hops J.

B. Satellite Coverage Model

The beam and satellite coverage have significant differences in terms of shape and size. For example, Starlink and Telesat use circularly shaped beams to form a circular satellite coverage, in which Starlink has a beam coverage area of about $2,800\ \mathrm{km}^2$ and Telesat has an adjustable beam coverage area of 960$\sim$246,000 km^2 [2]. Differently, OneWeb has fixed and highly elliptical beams with each size of about $75,000\ \mathrm{km}^2$, and the whole beams form an approximately rectangular satellite coverage area [2]. In fact, the beamforming technologies could form any desired satellite coverage shape and size. Thus, this paper mainly discusses six typical satellite coverage models, while the methodology could be followed by others.

To model the control structure (i.e., control domain) into a 2D graph considering the satellite coverage, we formulate the satellite coverage models consisted of one-hop coverage shape (OCS) and control domain shape (CDS) which are constructed as convex polygons with the maximum standard, that is with parameters around the Equatorial plane, to ensure the effective coverage for all latitudes. Specifically, the OCS is defined as a shape formed on the lattice graph by all LEO nodes directly covered by the controller, and the initial location of a non-LEO satellite is directly above the geometric center of its OCS. The length and width of OCS is n and m, respectively, where $n, m \geq 1$. The OCS is related to not only coverage shape, coverage angle, and inter-layer distance but also longitude and latitude differences between the adjacent LEO satellites. Assume the latitude and longitude differences between the adjacent LEO satellites around Equator are ΔL_a and ΔL_o, respectively. The minimum maximum spherical center angle of OCS in the direction of longitude and latitude is $\alpha_o = (n-1)\Delta L_o$ and $\alpha_a = (m-1)\Delta L_a$, respectively, which can associate with satellite coverage angle and inter-layer distance by the equation derived from Fig. 1(c):

$$\tan\frac{\beta}{2} = \frac{(R+\kappa_{leo})\sin(\alpha/2)}{(R+\kappa_{nleo}) - (R+\kappa_{leo})\cos(\alpha/2)}, \tag{1}$$

where R is the radius of the Earth and β is the coverage angle of a non-LEO satellite to LEO satellites. The CDS is defined as a shape formed on the lattice graph of all LEO

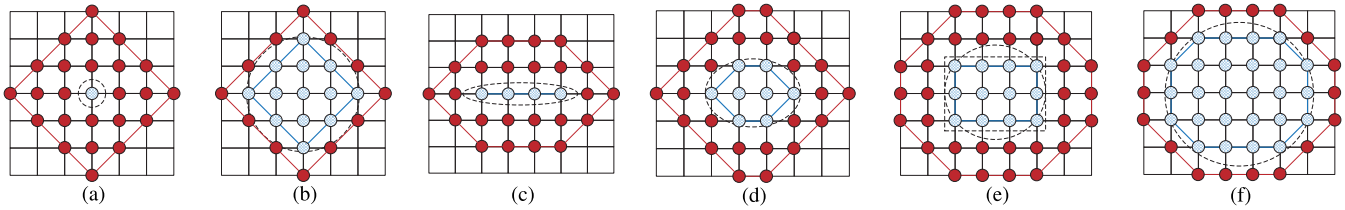

Fig. 2. Illustration of satellite coverage models for a) case I: point OCS and point/rhombic CDS, b) case II: rhombic OCS and rhombic CDS, c) case III: linear OCS and linear/hexagonal CDS, d) case IV: hexagonal OCS and hexagonal CDS, e) case V: rectangular OCS and rectangular/octagonal CDS, and f) case VI: octagonal OCS and octagonal CDS, in which blue-shading nodes represent LEO satellites that are one-hop distance away from its controller, red nodes represent LEO satellites that are more than one-hop distance away from its controller, blue edges form OCSs, red edges form CDSs, and dotted edges are possible satellite coverage edges. Note that same representation is applied on the later figures, we will not do repetitive specifications.

nodes controlled by a controller in J hops, where $J \geq 1$. Note that if $J = 1$, the CDS is equivalent to the OCS.

1) Case I — Point OCS and Point/Rhombic CDS: It is the simplest situation that a circular satellite coverage may form a 1×1 OCS (i.e., a point). The CDS shapes a rhombus when $J > 1$ or also a point when $J = 1$. From results in [34], we can derive the number of LEO satellites in the CDS of case I is:

$$V_I(J) = 2(J-1)^2 + 2(J-1) + 1. \tag{2}$$

For example, Fig. 2(a) illustrates case I with $J = 4$ and $V_I = 25$.

2) Case II — Rhombic OCS and Rhombic CDS: When the circular satellite coverage becomes larger or the LEO layer becomes denser, the case I may evolve to a rhombic OCS with $n = m$ and a rhombic CDS as shown in Fig. 2(b). This case can be seen as a variant of the case I with $J = J + (n-1)/2$. Thus, the number of LEO satellites in the CDS of case II can be derived by:

$$V_{II}(J) = V_I(J + \frac{n-1}{2}). \tag{3}$$

For example, Fig. 2(b) shows a 5×5 rhombus OCS and a rhombus CDS with $J = 2$ and $V_{II} = 25$.

3) Case III — Linear OCS and Linear/Hexagonal CDS: The LEO satellites covered by a non-LEO satellite with highly elliptical coverage may form a straight line in the lattice graph as shown in Fig. 2(c). According to the two elliptical focuses on the same row or column of the lattice graph, the line shape may be horizontal or vertical. Note that similar situations will also appear in the following cases. This paper mainly discusses the horizontal OCS (i.e., $n \geq m$), while the vertical OCS is just a right-angle rotation of the horizontal. Therefore, we have an $n \times 1$ linear OCS, and a linear CDS when $J = 1$ or a hexagonal CDS when $J > 1$. Further, the number of LEO satellites in the CDS of case III is given by:

$$V_{III}(n, J) = \begin{cases} n, & if\ J = 1; \\ n(2(J-1)+1) + 2(J-1)^2, & else. \end{cases} \tag{4}$$

Fig. 2(c) illustrates a 4×1 linear OCS and a hexagonal CDS with $J = 3$ and $V_{III} = 28$.

4) Case IV — Hexagonal OCS and Hexagonal CDS: When the satellite coverage extends vertically or the vertical distance between the adjacent LEO satellites reduces, the case III may evolve to a hexagonal OCS with $n - n_e = m - 1$ and a hexagonal CDS as shown in Fig. 2(d), where n_e is the number of LEO satellite nodes on the bottom edge of the OCS. The case IV can be seen as a variant of case III with $n = n_e$ and $J = J + (n - n_e)/2$. Thus, the number of LEO satellites in the CDS of case IV is:

$$V_{IV}(n, J) = V_{III}\left(n_e, J + \frac{n - n_e}{2}\right). \tag{5}$$

Fig. 2(d) shows a 4×3 hexagonal OCS and a hexagonal CDS with $n_e = 2$, $J = 3$ and $V_{III} = 32$.

5) Case V — Rectangular OCS and Rectangular/Octagonal CDS: On the LEO lattice graph, a circular or rectangular non-LEO satellite coverage may form a rectangular $n \times m$ OCS, and a rectangular CDS if $J = 1$ or an octagonal CDS if $J > 1$ as shown in Fig. 2(e). The number of LEO satellites in the CDS of case V is given by:

$$V_V(n, m, J) = nm + 2(J-1)(n + m + J - 2). \tag{6}$$

Fig. 2(e) illustrates a 4×3 rectangular OCS and an octagonal CDS with $J = 3$ and $V_V = 44$.

6) Case VI — Octagonal OCS and Octagonal CDS: When the satellite coverage expands or the LEO layer becomes denser, the case V may evolve to an octagonal OCS with $n - n_e = m - m_e$ and an octagonal CDS as shown in Fig. 2(f), where m_e is the number of LEO satellite nodes on the side edge of the CDS. The case VI can be seen as a variant of case V with $n = n_e$, $m = m_e$, and $J = J + (n - n_e)/2$. Thus, the number of LEO satellites in the CDS of case VI is:

$$V_{VI}(n, m, J) = V_V\left(n_e, m_e, J + \frac{n - n_e}{2}\right). \tag{7}$$

For example, Fig. 2(f) exhibits an octagonal OCS with $n = 6$, $n_e = 4$, $m = 5$, and $m_e = 3$, and an octagonal CDS that includes 44 LEO satellites with $J = 2$.

The above-mentioned satellite coverage models and concepts are the basis for further analysis for optimal space control network construction in the next section.

IV. Geometric Topology Analysis for the Optimal SCN Construction

In this section, we will analyze the optimal SCN construction of the first time slot to realize the ONCS. Based on the

modeling, the problem of the optimal SCN construction has been transformed into optimally placing CDSs into a 2D torus lattice, that is also to place the initial vertical projection points of the non-LEO satellites into a 2D torus lattice. With the analysis results, the constellation orbits can be determined by orbit geometry and determination [49], which is not our main contribution in this paper. Once we design the optimal SCN for the first time slot, the ONCS can be guaranteed through the proposed registration and handover schemes. The analysis develops from three OCS shapes: point, line, and rectangle.

A. Point-Shaped OCS

The OCSs of case I and II can be assigned to the point-shaped. Fortunately, the conditions of constructing the optimal space control networks for these cases can be derived from one of the conclusions in [34]: the best resource placement in a single-layer 2D-torus network is achieved when V can be divisible by the greatest common divisor (GCD) of N and M, mathematically expressed as $V|GCD\,(N, M)$, where $V = 2J^2+2J+1$ is the number of non-resource nodes that are at most J hops away from the resource node, and N and M are the dimensions of the torus [34]. Since the central LEO node in the point-shaped OCS is equivalent to the resource node in the single-layer 2D-torus network, we can derive the following theorem easily:

Theorem 1: The double-layer satellite networks with non-LEO satellite coverage of case I have the optimal space control network on the non-LEO satellite layer if and only if (iff) $J = J^*$, $N = N^*$, and $M = M^*$ satisfy

$$V_I\,(J^*)\,|\,GCD\,(N^*, M^*)\,, \tag{8}$$

where N^* and M^* are the optimal dimensions of the LEO satellite layer, and J^* is the optimal controllable hops of the non-LEO satellite controllers. Then, the number of required non-LEO satellites for constructing the optimal space control network is $N^*M^*/V_I(J^*)$.

Further, as mentioned before that case II can be seen as case I with $J = J + (n-1)/2$, we can deduce the corollary that:

Corollary 1: The double-layer satellite networks with non-LEO satellite coverage of case II have the optimal space control network iff $J = J^* - (n-1)/2$, $N = N^*$, and $M = M^*$, where N^*, M^*, and J^* are the optimal results in Theorem 1. Then, the number of required non-LEO satellites for constructing the optimal space control network is $N^*M^*/V_{II}(J)$.

As examples shown in Fig. 3(a) and 3(b), an optimal SCN can be achieved in a 5×5 torus lattice not only under satellite coverage of case I with $J = 2$ but also under satellite coverage of case II with $n = 3$ and $J = 1$. Both of which require five non-LEO satellites and have two selectable orbits (i.e., purple and green orbital structure in Fig. 3[2])

[2]Please note that the non-LEO layer orbits are mathematical construct that results from the theoretical treatment of the problem. Some orbits are physically impossible, such as purple orbits in Fig. 4(b).

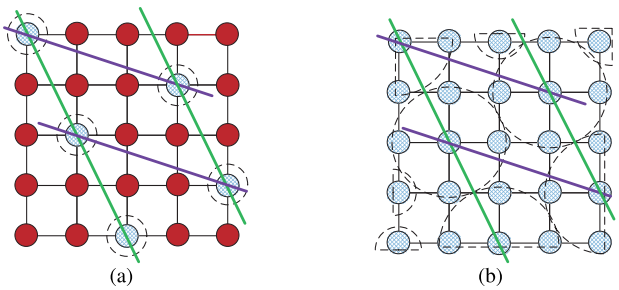

Fig. 3. Illustration of the optimal SCN and LEO layer configurations in a) a 5×5 torus lattice under non-LEO satellite coverage of case I with $J = 2$, and b) the same optimal configurations under satellite coverage of case II with $n = 3$ and $J = 1$. The purple line and green line are two selectable orbits for non-LEO satellites that are located at their intersections with coverage as dotted edges.

B. Line-Shaped OCS

The line-shaped OCS is related to satellite coverage models of case III and IV. First, we will introduce some basic concepts for the optimal SCN construction in current cases.

As shown in Fig. 4(a), C0 is the vertical projection of arbitrary non-LEO satellite controller on the 2D lattice graph, and also the benchmark for the placement of other controllers. In the Euclidean space $\mathbb{R}^2$, no matter where the other controllers place, they can all be delimited within an angle bounded by two vectors. Thus let vectors $\boldsymbol{r_1}$ and $\boldsymbol{r_2}$ starting at C0 be the two expansion boundaries for placing controllers. Then, considering the orbital regularity and the topological stability of non-LEO satellite layer, the placement of controllers both in the same and different orbits needs to have a uniform direction. Hence, the expansion boundaries are adopted as the two extension directions that are also the two selectable orbital directions for non-LEO satellite layer. Next, the controllers need to comply with continuous placement at a fixed distance interval both on $\boldsymbol{r_1}$ and $\boldsymbol{r_2}$ to ensure the CDSs of neighboring controllers are adjacent to avoid seams and overlaps, where 'adjacent' means that a one-hop connection exists between two LEO satellites belonged to different CDSs. Suppose that there are p_1 and p_2 controllers placed on $\boldsymbol{r_1}$ and $\boldsymbol{r_2}$ respectively when the optimal condition is achieved, in which C1 and C2 are the vertical projections of the first controller placed on $\boldsymbol{r_1}$ and $\boldsymbol{r_2}$, respectively. Further, we apply the horizontal and vertical phase differences $\Delta\Theta_1$ and $\Delta\Omega_1$ as well as $\Delta\Theta_2$ and $\Delta\Omega_2$, which are expressed by multiples of the phase difference $\Delta\theta$ and $\Delta\omega$ of the LEO layer lattice, to represent the distance intervals on $\boldsymbol{r_1}$ and $\boldsymbol{r_2}$, respectively. Besides, C3 is the vertical projection of a type of controller embedded between $\boldsymbol{r_1}$ and $\boldsymbol{r_2}$, and is located at the intersection of the two selectable orbital directions.

In this way, there are two key issues to be explored. One is the positional relationships between C0, C1, and C2 controllers, the other is the embedding and extension of other controllers.

1) Positional Relationships: The positional relationships between C0, C1, and C2 determines the extension directions and the distance intervals. We have the following lemmas to narrow the range of extension directions and conclude the positional relationships between C0, C1, and C2 controllers.

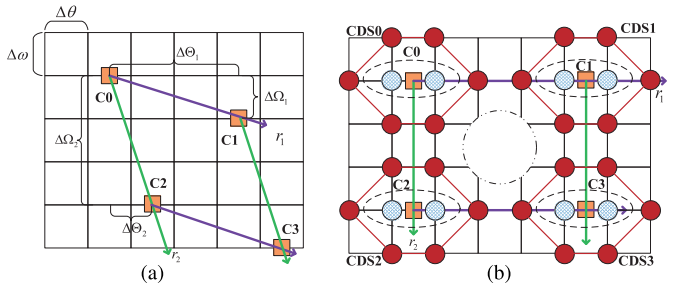

Fig. 4. Illustration of a) placement methods of non-LEO satellite controllers based on both the two extension directions: $\boldsymbol{r_1}$, $\boldsymbol{r_2}$ and the distance intervals on LEO and non-LEO layers represented by phase differences, and b) a possible positional relationship and the existing gap when $\boldsymbol{r_1} \perp \boldsymbol{r_2}$ for proof of Lemma 1 and 2.

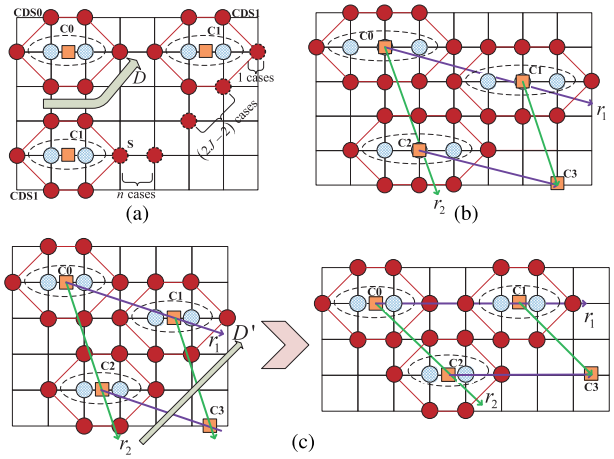

Fig. 5. Illustration of positional relationships for non-LEO satellite coverage of case III: a) CDS1 shifting direction $\boldsymbol{D}$ and $(2J+n-1)$ possible positions of its rightmost vertex during shifting, b) individual positional relationship when $n > 2$, and c) the variation of J possible positional relationships when $n = 2$.

Lemma 1: The angle of extension directions for placing hexagonal CDS is less than 90 degrees, that is $< \boldsymbol{r_1}, \boldsymbol{r_2} >< \frac{\pi}{2}$.

Proof: Consider a subspace $\mathcal{T}$ composed of a rectangular area in $\mathbb{R}^2$, where $\mathcal{T} = \{(x, y) \mid x, y \in \mathbb{R}, x \in [0, t_x), y \in [0, t_y)\}$. For an arbitrary $P_1, P_2 \in \mathcal{T}$ with $P_0(0, 0)$ as origin, the vector angle $< \boldsymbol{P_0P_1}, \boldsymbol{P_0P_2} >\leq \pi/2$ always holds. If $\mathcal{T}$ is a torus, then any $(x', y') \in \mathbb{R}^2$ can be mapped to $(x, y) \in \mathcal{T}$ by $x = x' - \lfloor |x'|/t_x \rfloor t_x$ and $y = y' - \lfloor |y'|/t_y \rfloor t_y$, due to cyclic features of the 2D torus. Thus (x', y') is equivalent to (x, y) for the torus. Then, assuming that controller C0 is located at P_0, no matter where C1 and C2 are located in $\mathbb{R}^2$, they can always be mapped into $\mathcal{T}$ by aforesaid method; so we have $< \boldsymbol{r_1}, \boldsymbol{r_2} >\leq \frac{\pi}{2}$. Further, if $\boldsymbol{r_1} \perp \boldsymbol{r_2}$, the hexagonal CDS3 cannot be embedded without overlaps or gaps for the reason that a two-node vertical gap between rightmost vertexes of CDSs along $\boldsymbol{r_2}$ cannot be filled by hexagonal CDS with one leftmost vertex as illustrated in Fig. 4(b). Thus $< \boldsymbol{r_1}, \boldsymbol{r_2} >< \frac{\pi}{2}$ holds. □

Lemma 2: The positional relationship between hexagonal CDSs of C1 and C2 is adjacent.

Proof: Based on Fig. 4(b) but without loss of generality, when the angle between $\boldsymbol{r_1}$ and $\boldsymbol{r_2}$ gradually decreases, there is always an unfillable gap between CDS1 and CDS2 until the two CDSs are adjacent, and then continuing to reduce the angle will cause them overlap. Thus, the hexagonal CDSs of controller C1 and C2 need to be kept adjacent, which also means that the hexagonal CDSs of C0, C1, and C2 are all adjacent. □

The above lemmas vastly restrict and reduce the possible positional relationships of C0, C1, and C2 controllers, thus we can enumerate all the positional cases of the three controllers.

Considering the symmetry of hexagonal CDS and taking CDS1 directly below CDS0 as the original case, all the relative positions of CDS1 to CDS0 can be obtained by shifting CDS1 along direction $\boldsymbol{D}$ which consists of any two adjacent edges of CDS0 as illustrated in Fig. 5(a). During the shifting process, CDS1 may be deployed below the bottom edge (i.e., n cases with $\Delta\Theta_1 = 0, \ldots, n-1$), beside the bevel edge (i.e., $(2J - 2)$ cases), and beside the side edge (i.e., 1 case with $\Delta\Omega_1 = 0$) of CDS0. Then, we have the following lemma:

Lemma 3: For the line-shaped OCS with hexagonal CDS, when $n = 2$*, the controller C0, C1, and C2 have J positional relationships renumbered as case* $i = 1, \ldots, J$*; when* $n > 2$*, they have only one positional relationship renumbered as case* $i = 1$.

Proof: In all $(2J + n - 1)$ cases, the first n cases could be removed due to repetition or existing gaps/overlaps; the remaining $(2J - 1)$ cases are highly repeated and can be integrated into J possible cases. When $n = 2$, the J cases are all effective; but when $n > 2$, only one case is valid. To obtain detailed reasoning, please see Appendix A. □

For example but without loss of generality, Fig. 5(b) illustrates the individual positional relationship with $n = 3$ and $J = 1$. Fig. 5(c) exhibits the J effective positional relationships with $n = 2$ and $J = 2$, in which all the cases can be entirely obtained by shifting CDS1 and CDS2 along $\boldsymbol{D'}$. During the whole shifting process, the top edge of the CDS2 is always flush with the bottom edge of CDS1. The positional relationship before shifting is shown in the left graph of Fig. 5(c), where the central row of CDS1 is flush with the bottom edge of CDS0. Here, the $\Delta\Theta_1$ and $\Delta\Theta_2$ have minimum values, but $\Delta\Omega_1$ and $\Delta\Omega_2$ are maximum. After $(J - 1)$ shifts, the case comes to the right graph of Fig. 5(c), where the central rows of both CDS0 and CDS1 are flush. Here, the $\Delta\Theta_1$ and $\Delta\Theta_2$ have maximum values, but $\Delta\Omega_1$ and $\Delta\Omega_2$ are minimum.

By these lemmas, we can further deduce the following conclusions about distance intervals between neighbor controller by applying phase differences:

$$\begin{aligned} \Delta\Theta_1 &= (n + J + i - 2)\,\Delta\theta = g_1\Delta\theta, \\ \Delta\Omega_1 &= (J - i)\,\Delta\omega = g_2\Delta\omega, \\ \Delta\Theta_2 &= i\Delta\theta = g_3\Delta\theta, \\ \Delta\Omega_2 &= (2J - i)\,\Delta\omega = g_4\Delta\omega, \end{aligned} \tag{9}$$

where $i = 1, \ldots, J$ when $n = 2$, and $i = 1$ when $n > 2$. These formulae also indirectly represent the orbital relationships between the two satellite layers. If the orbital parameters of

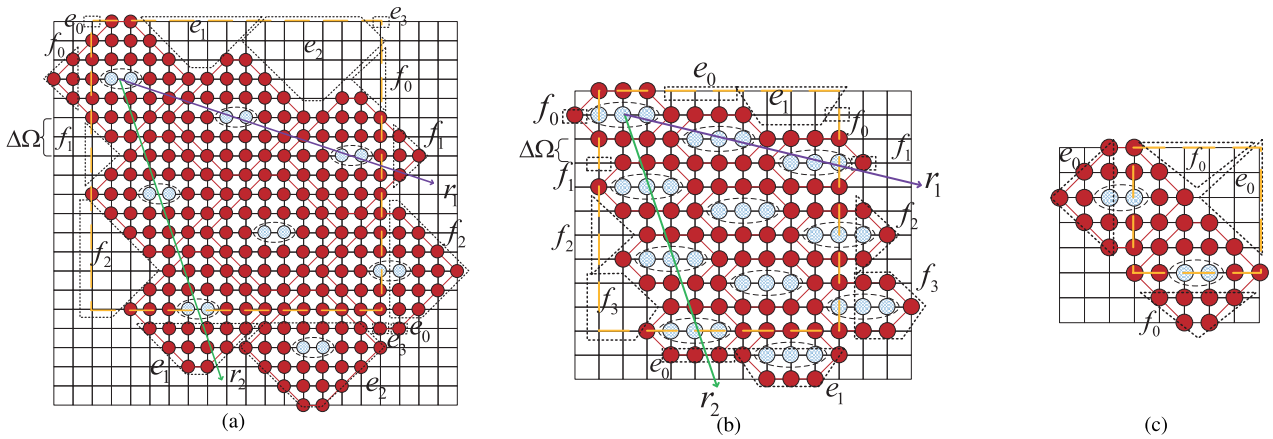

Fig. 6. Illustration of subregions and the optimal SCN and LEO layer configurations of case III with a) $n = 2$, $J = 4$, and $i = 2$, b) $n = 3$, $J = 1$, and $i = 1$, and c) $n = 2$, $J = 3$, and $i = 3$, where the yellow dotted boxes are the lattice graphs of optimal LEO layer configuration.

LEO satellites are known in detail, the two selectable orbits of non-LEO satellites can be derived geometrically.

2) Embedding and Extension of Other Controllers: After getting the positional relationships of the first three controllers, the subsequent problems are how to ensure the seamless and non-overlapping embedding of the unsmooth CDSs and how many CDSs should be placed on the extension directions to satisfy the graph can be filled into a quadrilateral torus lattice.

First, we will introduce some basic definitions. We have mentioned that the number of controllers to be placed on $\boldsymbol{r_1}$ and $\boldsymbol{r_2}$ are p_1 and p_2, respectively, excluding controller C0. Then, suppose another variable $p_2' \leq p_2 + 1$, where the i^{th} row of the ${p_2'}^{th}$ extended CDS (i.e, excluding CDS0) along $\boldsymbol{r_2}$ and the middle row of the p_1^{th} extended CDS along $\boldsymbol{r_1}$ are on the same horizontal loop. To intuitively understand these definitions, we take Fig. 6(a) with $n = 2$, $J = 4$, and $i = 2$ as an example, where three controllers are placed on both $\boldsymbol{r_1}$ and $\boldsymbol{r_2}$ (i.e., $p_1 + 1 = 3$ and $p_2 + 1 = 3$), and the second (i.e., i^{th}) row of the first (i.e., ${p_2'}^{th}$) extended CDS along $\boldsymbol{r_2}$ is on the same horizontal loop as the middle row of the second (i.e., ${p_1}^{th}$) extended CDS along $\boldsymbol{r_1}$, that is $p_2' = 1$.

Subsequently, we consider the embedding problem and have the following lemma:

Lemma 4: In the above effective cases except case $i = J$, the embedded controllers with hexagonal CDS can always be embedded without overlaps and gaps.

Proof: Regarding $\boldsymbol{r_1}$ and $\boldsymbol{r_2}$ as two coordinate axes with C0 as origin, the other controllers on $\boldsymbol{r_1}$ and $\boldsymbol{r_2}$ can be represented as $(x_r, 0), x_r = 1, \ldots, p_1$, and $(0, y_r), y_r = 1, \ldots, p_2$. For arbitrary embedded controller at (x_r, y_r) sandwiched between line $\iota_{r_2=y_r-1}$ and $\iota_{r_1=x_r-1}$, it has two neighbor controllers at $(x_r, y_r - 1)$ and $(x_r + 1, y_r - 1)$ on $\iota_{r_2=y_r-1}$ as well as two neighbor controllers at $(x_r - 1, y_r)$ and $(x_r - 1, y_r + 1)$ on $\iota_{r_1=x_r-1}$. Letting controller at $(x_r, y_r - 1)$ roled as C0, due to $\iota_{r_1=x_r} // \boldsymbol{r_2}$ and $\iota_{r_2=y_r-1} // \boldsymbol{r_1}$, the embedded controller to the two neighbor controllers on $\iota_{r_2=y_r-1}$ enable to construct the basic positional relationship, where the embedded controller acts as C2. Similarly, the embedded controller acted as C1 can also consist of the basic positional relationship with the two neighbor controllers on $\iota_{r_1=x_r-1}$. Therefore, arbitrary embedded controller and its CDS are adjacent with neighbor controllers and CDSs. As for case $i = J$, we will see later that this is a particular case that only two controllers could achieve the optimal SCN construction, so that no embedding issues are with case $i = J$. □

Next, the conditions for the optimal SCN construction and the extension methods will be given in the form of theorem. Meanwhile, the recommendations about the optimal LEO and non-LEO layer configurations are included.

Theorem 2: The double-layer satellite networks with non-LEO satellite coverage of case III have the optimal space control network on non-LEO satellite layer with following conditions and conclusions:

1) When $J = 1$, then

- *$(N/n) \in \mathbb{N}^*$ is the only needed condition for constructing the optimal space control network.*
- *The optimal structure of LEO layer is $N^* \times M^*$, where $N^* = k_1 n, k \in \mathbb{N}^*$ and $M^* = k_2 \in \mathbb{N}^*$.*
- *The number of the non-LEO satellites is $k_1 n k_2$.*

2) When $J > 1$, then

- *If $i \neq J$, then $\forall i$, $\exists i$ that makes $p_2 = ((n + J - 2)/g_3) \in \mathbb{N}$; meanwhile, $\exists p_1, p_2' \in \mathbb{N}$ satisfy $(p_1 - 1) g_2 = i + (p_2' - 1) g_4$ and $p_2' = (J - i)/i$; Else, the optimal condition does not hold.*
- *If $i = J$, then the optimal condition always holds by only two controllers.*
- *With above p_1, p_2, and p_2', the double-layer satellite networks with non-LEO satellite coverage of case III enable to construct the optimal space control network when the LEO structure is $N^* \times M^*$, where*

$$N^* = \begin{cases} k_1 (2J), & i = J; \\ k_1 (g_1 p_1 \\ \quad + (n + (J - 1 - g_3 p_2') + (i - 1))), & else, \end{cases} \tag{10}$$

and

$$M^* = \begin{cases} k_2 (g_4 + J), & i = J; \\ k_2 (g_4 p_2 + J), & else, \end{cases} \tag{11}$$

in which $k_1, k_2 \in \mathbb{N}^*$ are extension factors.

TABLE I
EXAMPLES FOR THEOREM 2 ($J > 1$)

$n \times m$	2×1	2×1	2×1	2×1	2×1	2×1	2×1	3×1	3×1	3×1	4×1	5×1
J	3	3	4	4	4	5	5	2	3	4	3	3
V_{III}	18	18	32	32	32	50	50	11	23	39	28	33
i	1	3	1	2	4	1	5	1	1	1	1	1
g_1	4	6	5	6	8	6	10	4	5	6	6	7
g_2	2	0	3	2	0	4	0	1	2	3	2	2
g_3	1	3	1	2	4	1	5	1	1	1	1	1
g_4	5	3	7	6	4	9	5	3	5	7	5	5
p_1	4	-	6	2	-	8	-	2	4	6	4	4
p_2	3	-	4	2	-	5	-	3	4	5	5	6
p_2'	2	-	3	1	-	4	-	1	2	3	2	2
$N^*(k_1 = 1)$	18	6	32	16	8	50	10	11	23	39	28	33
$M^*(k_2 = 1)$	18	6	32	16	8	50	10	11	23	39	28	33
Number of controllers	18	2	32	8	2	50	2	11	23	39	28	33

- *The number of non-LEO satellite controllers is*:

$$\frac{N^* \times M^*}{V_{III}(J)} = \begin{cases} 2k_1k_2, & i = J; \\ (p_1\,(p_2+1)+n)\,k_1k_2, & else. \end{cases} \quad (12)$$

Proof: a) When $J = 1$, as long as horizontal dimension of LEO lattice can be divisible by n, the optimal SCN can be constructed. Then, the rest conclusions can be simply derived, so that we will not elaborate and just focus on cases of $J > 1$.

b) When $J > 1$ and $i \neq J$, please see Appendix B.

c) When $J > 1$ and $i = J$, the optimal space control network can always be achieved by two controllers, as illustrated in Fig. 6(c), where the LEO structure under optimal condition can be directly derived by illustration, that is $N^* = 2J$ and $M^* = g_4 + J$.

d) Then, we can derive the number of non-LEO satellites under optimal condition is $N^* \times M^*/V_{III}(J)$. It can also be given by another form by analyzing the non-LEO layer configuration. When $i \neq J$, the number of orbits along $\boldsymbol{r_2}$ directions is $(p_1 + 1)$, in which each of the first p_1 orbits has (p_2+1) controllers and the last orbit has n controllers. Therefore, the number of non-LEO satellites is $(p_1\,(p_2 + 1) + n)$. When $i = J$, two controllers are enough.

e) Finally, a basic optimal SCN (BOS) can be obtained through proven conclusions. To be applied into MSCs, the horizontal or/and vertical extension/expansion of the BOS can be seen as the increase of both the number of orbits and controllers along extension directions. By Lemma 4, we know that the extension of CDSs along $\boldsymbol{r_1}$ and $\boldsymbol{r_2}$ will not bring gaps/overlaps and embedding problems. Thus the vacant subregions to be filled can be directly filled by extended BOSs which also bring new vacant subregions with the same shapes. These new unfilled subregions can be filled by the opposite graph as proved before. Therefore, the network scale can be extended by $k_1 \in \mathbb{N}^*$ times horizontally or/and $k_2 \in \mathbb{N}^*$ times vertically based on BOS to form an MSC. □

As example to verify our conclusions, Table I shows all significant values for optimal SCN construction when $J > 1$.

As mentioned in section III, the satellite coverage model of case IV is a variant of case III, thus the conclusions of its optimal SCN construction can be directly derived as follows, which will no longer be proved.

Corollary 2: The double-layer satellite networks with non-LEO satellite coverage of case IV have the optimal space control network and corresponding optimal configurations of both LEO and non-LEO layer, which also follows the theorem 2 with $n = n_e$ and $J = J + (n - n_e)/2$.

C. Rectangular-Shaped OCS

The rectangular-shaped OCS includes satellite coverage models of cases V and VI. These cases still follow similar lemmas as Lemma 1 and Lemma 2, and the ideas of their proofs are identical. However, the positional relationships and the optimal conclusions have some changes.

Similarly, all the relative positions of CDS1 to CDS0 can be obtained by shifting CDS1 along direction $\boldsymbol{D}$ which consists of any two adjacent edges of CDS0 as illustrated in Fig. 7(a). During the shifting process, CDS1 may be placed below the bottom edge (i.e., n cases of $\Delta\Theta_1 = 0, \ldots, n-1$), beside the bevel edge (i.e., $2J - 2$ cases), and beside the side edge (i.e., m cases of $\Delta\Omega_1 = m - 1, \ldots, 0$) of CDS0. Then, we have the following lemma:

Lemma 5: For the rectangular-shaped OCS with octagonal CDS, when $n = 2$ and $m = 2$, the controller C0, C1, and C2 have 2 positional relationships renumbered as $I = 0$ and $I = 1$; when $n > 2$ and $m = 2$, they have only 1 positional relationship renumbered as $I = 1$; when $n > 2$ and $m > 2$, there is no satisfied positional relationship.

Proof: In the first n cases, when $\Delta\Theta_1 = 0$, a two-node vertical gap is needed to be filled between the rightmost edge of CDS0 and CDS1. Therefore, if $m = 2$, an effective positional relationship renumbered as $I = 1$ is obtained as shown in Fig. 7(c) and 7(d) for examples. Note that this case is also the second case of the undiscussed $(2J - 2)$ cases, where CDS1 is beside the bevel edge of CDS0. The remaining $(n-1)$ cases are all not feasible for the reason that a one-node vertical gap exists between the rightmost edge of CDS0 and the top edge of CDS1, which cannot be filled by a CDS with $m \geq 2$.

In the last m cases, the first case is with $\Delta\Omega_1 = 0$, where a two-node horizontal gap exists between the

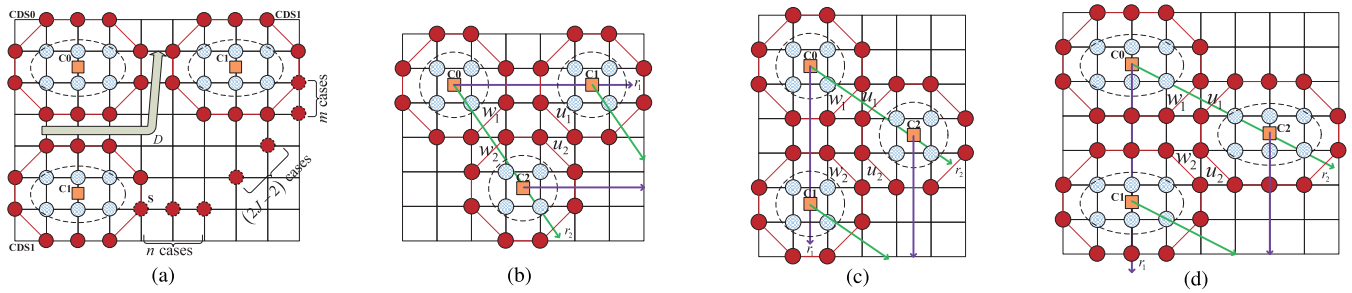

Fig. 7. Illustration of positional relationships for satellite coverage of case V: a) CDS1 shifting direction $\boldsymbol{D}$ and $(2J+n+m-2)$ possible positions of its one rightmost vertex during shifting, b) and c) the two positional relationships when $n=2$ and $m=2$, and d) the individual positional relationship when $n>2$ and $m=2$.

$(m+J)^{th}$ rows of both CDS0 and CDS1. Although the gap can be filled by CDS with $n=2$, it can be seen that this feasible case is a duplicate of the first case in the undiscussed $(2J-2)$ cases. A related example is illustrated in Fig. 7(b). Besides, the remaining $(m-1)$ cases are all not feasible, because a one-node horizontal gap between the bottom edge of CDS0 and the side edge of CDS1 is impossible to be filled by CDS with $n \geq 2$.

Except for the two repeated cases in the undiscussed $(2J-2)$ cases, other cases are all unavailable due to a one-node gap existing between CDS0 and CDS1 constantly.

Lastly, due to parallel features of adjacent bevel edges that belong to different CDSs, that is $w_1 // u_1$ and $w_2 // u_2$ shown in Fig. 7(b)-7(d), the CDSs in the above feasible cases can still be effectively placed without overlaps and gaps as J increases. □

Up to two available positional relationships make it easy to obtain the conditions for constructing the optimal SCN under the rectangular satellite coverage model. Also, we will see later that there is no embedding problem in these cases. The conditions for optimal SCN construction and the recommendations for the optimal LEO and non-LEO configurations are as follows:

Theorem 3: The double-layer satellite networks with non-LEO satellite coverage of case V have the optimal space control network on the non-LEO satellite layer with following conditions and conclusions:

1) When $J=1$, then

- *The conditions for constructing the optimal space control network are $(N/n) \in \mathbb{N}^*$ and $(M/m) \in \mathbb{N}^*$.*
- *The optimal LEO structure is $N^* \times M^*$, where $N^* = k_1 n, k_1 \in \mathbb{N}^*$ and $M^* = k_2 m, k_2 \in \mathbb{N}^*$.*
- *The number of non-LEO satellite controllers is $k_1 k_2 nm$.*

2) When $J>1$, then

- *Only two CDSs are needed to achieve the optimal space control network.*
- *For case $I=0, n=2, m=2$, the optimal LEO structure is $N^* \times M^*$, where $N^* = k_1(g_1+J), k_1 \in \mathbb{N}^*$, and $M^* = k_2(g_2+J+m-1), k_2 \in \mathbb{N}^*$. The number of non-LEO satellite controllers is $2k_1k_2$.*
- *For case $I=1, n \geq 2, m=2$, the optimal LEO structure is $N^* \times M^*$, where $N^* = k_1(g_1+J+n-1), k_1 \in \mathbb{N}^*$, and $M^* = k_2(g_2+J), k_2 \in \mathbb{N}^*$. The number of non-LEO satellite controllers is also $2k_1k_2$.*

Proof: When $J=1$, as long as the length and width of the rectangular CDS are the divisors of the length and width of the LEO layer lattice respectively, the optimal SCN construction is achieved, and then the rest conclusions can be easily derived.

When $J>1$, the situation becomes less complicated due to the drastic reduction in feasible positional relationships. With the help of Fig. 8(a) and Fig. 8(b) but without loss of generality, both of the two feasible positional relationships require only two CDSs to form a torus lattice. The distance intervals of the two CDSs are:

$$\begin{aligned} \Delta\Theta_1 &= (n+J+I-2)\,\Delta\theta = g_1\Delta\theta, \\ \Delta\Omega_1 &= (m+J-I-1)\,\Delta\omega = g_2\Delta\omega. \end{aligned} \tag{13}$$

N^* and M^* are the number of LEO satellites contained in the horizontal and vertical edge of optimal torus lattice, whose specific components are given by the illustrations in Fig. 8. Similar to Theorem 2 and its proof, the structure of LEO layer could be further expanded for MSC with horizonal or/and vertical extension/expansion by k_1 or/and k_2 times of the BOS. □

To verify the conclusions, Table II lists some examples of Theorem 3. Then, since the satellite coverage model of case VI can be obtained by reformulating case V, the conclusions of optimal SCN construction for the last satellite coverage model can be directly derived as follows:

Corollary 3: The double-layer satellite networks with non-LEO satellite coverage of case VI have the optimal space control network and corresponding optimal configurations of both LEO and non-LEO layer, which also follows the theorem 3 with $n=n_e$, $m+m_e$, and $J=J+(n-n_e)/2$.

As a result, the conclusions not only provide the optimal number of LEO satellites and non-LEO satellite controllers but also illustrates some possible orbital relationships between the two layers, which can facilitate to derive the specific structures of the double satellite layers if some precise parameters of non-LEO satellites (e.g., altitude, controllable hops, and satellite coverage angle) and LEO satellites (e.g., inclination, altitude) are determined. In practical applications, for LEO satellite constellations that have been launched or completed, the appropriate SCN structures can be approximately selected according to the LEO-layer configurations. For constellations

TABLE II
EXAMPLES FOR THEOREM 3 ($J > 1$)

$n \times m$	2×2	2×2	2×2	2×2	2×2	2×2	3×2	3×2	3×2	4×2	5×2
J	2	2	3	3	4	4	2	3	4	3	3
V_V	12	12	24	24	40	40	16	30	48	36	42
I	0	1	0	1	0	1	1	1	1	1	1
g_1	2	3	3	4	4	5	4	5	6	6	7
g_2	3	2	4	3	5	4	2	3	4	3	3
$N^*(k_1 = 1)$	4	6	6	8	8	10	8	10	12	12	14
$M^*(k_2 = 1)$	6	4	8	6	10	8	4	6	8	6	6
Number of controllers	2	2	2	2	2	2	2	2	2	2	2

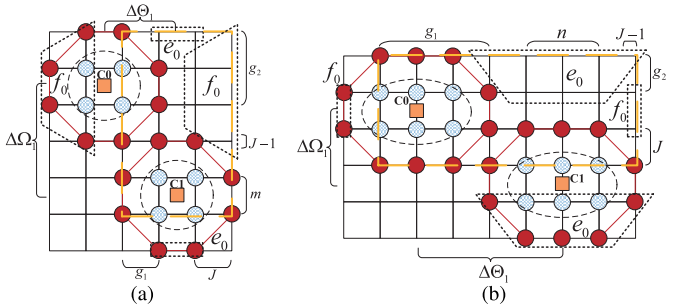

Fig. 8. Illustration of subregions and optimal SCN and LEO layer configurations of case V with a) $n = 2$, $m = 2$, and $J = 2$, and b) $n = 3$, $m = 2$, and $J = 2$, where the yellow dotted boxes are the lattice graphs of optimal LEO-layer configuration.

still at initial period, our conclusions can provide effective guidance for the configurations of both LEO satellite constellation and non-LEO satellite controllers.

V. CONTROL SCENARIOS AND RESULTS

To demonstrate the temporal effectiveness of the proposed optimal SCN, we first evaluate the control delays (mainly for propagation delay [50]) in the three common satellite network control scenarios (i.e., signaling distribution, new node participation, and fault discovery) to investigate the relationships among several typical network variables (i.e., control delay, LEO constellation scale, as well as controllable hops, coverage angle, and altitude of non-LEO satellites) according to the derived conclusions.

A. Control Scenarios and Control Delays

1) Signaling Distribution: Signaling distribution is a process that the controller distributes signaling to its controlled LEO satellites. This scenario is a crucial component of numerous network control processes, such as routing maintenance, location update, and resource scheduling decisions, and also a key factor affecting the performance of the whole control procedures. The control delay of signaling distribution is the average propagation delay during all non-LEO satellite controllers distributing signaling to each controlled LEO satellite.

2) New Node Participation: Due to the limited lifetime of satellites and the demand for the constellations to be expanded in stages, the controllers need to cope with the supplement or replacement of new satellites. In this scenario, the SCC linked with GSs first informs the non-LEO satellite controllers of the new satellite information that is then broadcasted to the LEO layer to facilitate building new neighbor relationships. The control delay of this process consists of the average propagation delay from ground to non-LEO satellite controllers and the signaling distribution delay for building new neighbor relationships.

3) Fault Discovery: The radiation of cosmic rays, asteroid collisions, and equipment lifetime are all reasons for satellite failures. If the fault is not discovered and dealt with in time, it will cause many problems, such as data forwarding failure, continuous retransmission, and inappropriate control decisions, so rapid fault response is crucial. Normally, the satellite reports the status and problem to its controller periodically, and then the controller will perceive the potential or existing failures and inform all the controlled LEO satellites of the failure information to prevent the malfunctioning satellite from appearing on the data transmission path. The control delay of fault discovery includes the propagation delay for status reporting from LEO satellites to their non-LEO controllers and the signaling distribution delay for failure information distribution.

B. Numerical Results

In this section, MEO satellites are equipped with controller payload to form the optimal SCN. The numerical results can be obtained as follows. Given LEO layer configurations, all possible combinations of the optimal SCN configurations, OCSs, and controllable hops can be derived by our conclusions. Then, according to the design constraints of MEO satellites in altitude, coverage angle, and coverage shape, the feasible OCSs can be obtained by filtering out the inappropriate combinations. Finally, we can get the optimal SCN configurations with different controllable hops of MEO controllers. However, there is a high correspondence between the optimal results and the variables, making it very hard to fix some control variables to demonstrate the interrelationships of the others. Thus, we note that some independent variables cannot be fixed in the results, but their values approximate to a certain common number, which can ensure the correctness of the result trends.

1) Fixed OCS: This part mainly explores the variation tendency of the optimal number of required controllers as well as the signaling distribution delays with the controllable hops and LEO constellation scale under a fixed OCS (i.e., fixed coverage angle and altitude of MEO satellites). Fig. 9 shows

TABLE III
VARIATION OF CONTROL DELAYS (ms) WITH LEO CONSTELLATION SCALE AND CONTROLLABLE HOPS

Variables [Fixed variables]	≈ LEO scale [J = 4]						Controllable hops [≈10000 LEO satellites]				
	4000	6000	8000	10000	12000	14000	2	3	4	5	6
Signaling distribution	25.53	24.86	24.59	24.43	24.32	24.23	23.31	23.89	24.43	25.13	25.70
New node participation	53.51	52.83	52.57	52.40	52.29	52.21	51.29	51.87	52.40	53.11	53.67
Fault discovery delay	51.06	49.72	49.18	48.85	48.63	46.47	46.62	47.78	48.85	50.27	51.40

TABLE IV
VARIATION OF CONTROL DELAYS (ms) WITH MEO SATELLITE ALTITUDES AND MEO SATELLITE COVERAGE ANGLES (≈8000 LEO SATELLITES)

Variables [Fixed variables]	Altitude (km) [Coverage angle=20deg]				Coverage angle (deg) [Altitude=8000km]			
	4000	6000	8000	10000	10	20	30	40
Signaling distribution	11.66	18.10	24.67	32.09	24.75	24.80	25.12	25.44
New node participation	25.65	39.09	52.64	67.06	52.73	52.78	53.09	53.41
Fault discovery delay	23.33	36.21	49.33	64.19	49.50	49.61	50.23	50.88

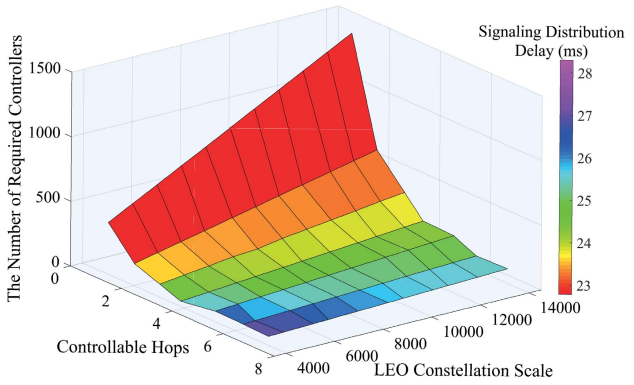

Fig. 9. Variation tendency of the optimal number of required controllers as well as signaling distribution delays with the controllable hops and LEO constellation scale under fixed OCS of $n = 5$ and $m = 2$, in which the altitude and coverage angle of MEO satellites is fixed $\kappa_{nleo} = 8000$km and $\beta = 20\,\deg$ respectively, and the altitude of LEO satellites is $\kappa_{leo} = 1200$km.

the results under a fixed OCS with $n = 5$, $m = 2$, $\kappa_{nleo} = 8000$km, and $\beta = 20\,\deg$. On the one hand, as the controllable hops increase, the number of controllers decreases rapidly and then steadily, which means that the gain in the number of controllers is gradually weakening. Meanwhile, when the LEO constellation scale grows, the number of required controllers raises sharply at small J and gently at large J. On the other hand, from the temperature map of signaling distribution delay, it can be observed that both the reduction of LEO satellite constellation scale and the increase of controllable hops will worsen the delays.

As a result, we have an interesting finding that blindly improving the controllable hops will not facilitate the rapid and continuous decline of the optimal number of required controllers. Most importantly, there exists a tradeoff between the number of controllers and control delays. In practice, we can set appropriate controllable hops according to the delay demands and the LEO constellation scale to make a tradeoff. As comparisons, table III shows the variation of control delays with the LEO satellite constellation scale and controllable hops in the three common control scenarios.

2) Variable MEO Satellite Altitudes: In this part, we fix the coverage angle and controllable hops to study the impact of MEO satellite altitudes on control delays as well as the optimal number of required controllers, as shown in Fig. 10(a) and Fig. 10(b). Since the increase in MEO altitude will affect the OCS, we select the results of larger OCS for higher altitudes. Under the same LEO constellation scale, the lower altitudes the MEO satellites deploy, the more the controllers are required, and the lower the signaling distribution delays. At the same MEO satellite altitude, the optimal number of required controllers increases as the LEO constellation scale rises, while the signaling distribution delay decreases smoothly. Although higher altitudes could expand OCS and effectively reduce the controller quantity, the unavoidable long distance and high delay may not satisfy the demand for network control, thus bringing a tradeoff between the MEO satellite altitude and the control delay performance. Moreover, the delay variations of the three common control scenarios with MEO satellite altitudes are compared in the left part of table IV, where we can observe that the altitude has a significant impact on the control delays.

3) Variable MEO Satellite Coverage Angles: The MEO satellite coverage angle is another important factor affecting the distance between MEO and LEO satellites. In this part, the changes in the optimal number of required controllers and control delays are explored under the fixed MEO satellite altitude and controllable hops. As shown in Fig. 10(c) and 10(d), the rising of MEO satellite coverage angle expands the OCS so that the optimal number of required controllers under the same LEO constellation scale is reduced, while the signaling distribution delay becomes worse due to elongated link distance. With the same MEO satellite coverage angle, the signaling distribution delay improves with the LEO constellation scale. Moreover, Table IV compares the delay variations of the three common control scenarios with MEO satellite coverage angles. We observe that the variable trends of the control delays listed in the right part of Table IV are more gradual than the left. A similar phenomenon can also be found by comparing Fig. 10(b) and 10(d), which means the impact of the variation of MEO satellite coverage angle on the control

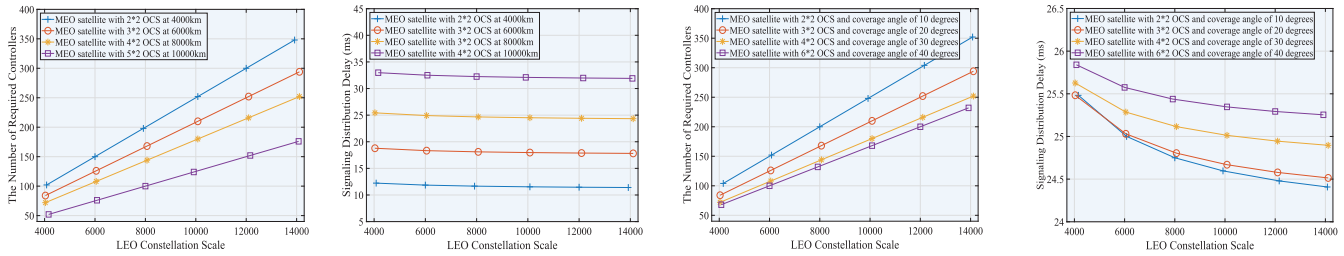

Fig. 10. Variation of a) the optimal number of required controllers and b) signaling distribution delays with the MEO satellite altitude and LEO satellite constellation scale under fixed MEO satellite coverage angle $\beta = 20\,\text{deg}$ and static controllable hops $J = 4$, as well as the variation of c) the optimal number of required controllers and d) signaling distribution delays with the MEO satellite coverage angle and LEO constellation scale under fixed MEO satellite altitude $\kappa_{nleo} = 8000\text{km}$ and static controllable hops $J = 4$. Note that the altitude of LEO satellites is all $\kappa_{leo} = 1200\text{km}$.

TABLE V
FOUR FEASIBLE OSCNS AND SIGNALING DISTRIBUTION DELAYS FOR ONEWEB SYSTEM

OSCN parameters									Average/maximum delays (ms) with varying MEO altitudes			
$n \times m$	J	V	I	k_1	k_2	N^*	M^*	$\frac{N^*M^*}{V}$	5000km	10000km	15000km	20000km
2×2	2	12	1	3	10	$6k_1$	$4k_2$	60	15.35 / 18.98	31.88 / 35.47	48.51 / 52.08	65.16 / 68.72
8×2	2	36	1	1	10	$18k_1$	$4k_2$	20	17.71 / 28.15	33.54 / 42.52	49.92 / 58.27	66.44 / 74.46
6×2	4	72	1	1	5	$18k_1$	$8k_2$	10	21.41 / 32.60	37.39 / 47.62	53.83 / 63.73	70.39 / 80.13
5×2	5	90	1	1	4	$18k_1$	$10k_2$	8	23.24 / 35.83	39.35 / 51.23	55.84 / 67.48	72.42 / 83.94

delay is relatively more minor compared to the MEO satellite altitude.

To conclude, a larger satellite coverage angle and a higher MEO satellite altitude can reduce the optimal number of required controllers but worsen the delays. Besides controllable hops, we can also design an appropriate coverage angle and altitude of MEO satellites to balance the optimal number of controllers and control delays.

C. Optimal SCN (OSCN) Design for OneWeb

To show the effectiveness of the proposed ONCS, we further design an OSCN for OneWeb system. The OneWeb system consists of 720 LEO satellites uniformly distributed in 18 circular orbital planes at an altitude of 1200 kilometers, each plane inclined at 87.9° [2].

We assume that the non-LEO satellite coverage obeys rectangular-shaped OCS and octagonal CDS so that the OSCN can be designed by Theorem 3. The four feasible OSCNs for OneWeb system are shown in Table V, where the specific OSCN parameters are given. Since all the BOSs are based on the case $I = 1$, the inclination of non-LEO satellite orbits could be the same as that of the OneWeb satellites. Thus, the OSCN has $2k_1$ orbits and k_2 satellites per orbit.

Table V also shows the average and maximum signaling distribution delays with varying MEO altitudes, where the number of controllers is inversely proportional to the control delay but directly proportional to the construction cost, and the smaller number of controllers has a significant oscillation in the control delay due to the required large CDS.

VI. CONCLUSION

In this paper, we focus on designing the ONCS by constructing an optimal SCN on the non-LEO satellite layer, and obtain an interesting finding in the tradeoff between the optimal number of controllers and control delays. To minimize the number of controllers under guaranteed control performance conditions, the conclusions with closed-form formulae are derived, which can obtain both the conditions for the optimal SCN construction and the overall network configurations given satellite coverage features and controllable hops. By expanding the basic optimal cases, a mega satellite constellation can be constructed for future space Internet and integrated networks.

APPENDIX A
PROOF OF LEMMA 3

a) In all $(2J + n - 1)$ cases, the first n cases could be removed. Specifically, when $\Delta\Theta_1 = 0$, a two-node vertical gap is needed to be filled between the rightmost vertexes of CDS0 and CDS1, but hexagonal CDS has only one side vertex, so there is no suitable position for CDS2 being adjacent to both CDS0 and CDS1. A general example can be referred to in Fig. 5(a). When $\Delta\Theta_1 = 1$, the position of CDS1 is similar to the position of CDS2 shown in Fig. 5(b) and left Fig. 5(c). Accordingly, the only available position for CDS2 is just like the position of CDS1 in the figures, so these are repeated cases. Further, the cases of $\Delta\Theta_1 = 2, \ldots, n-1$ only exist when $n > 3$, but to ensure CDS2 to be adjacent to CDS0, the bottom edge of CDS2 will overlap the top edge of CDS1.

b) Then, the remaining $(2J - 1)$ cases are highly repeated. Specifically, the $c^{th}, c = 1, \ldots, J-1$, case is equivalent to the $(c+J)^{th}$ case by swapping CDS1 and CDS2, and the J^{th} case is equivalent to the above-mentioned case of $\Delta\Theta_1 = 1$. Using the right part of Fig. 5(c) as example but without loss of generality, it shows CDS1 is beside the rightmost vertex of CDS0, which is the last case of the remaining $(2J-1)$ cases, namely $c = J - 1$. Then swapping positions of CDS1 and

CDS2, we can get the c^{th} case, where CDS1 is beside the bevel edge of CDS0. Thus the last J cases become our focus and are renumbered as the case $i = 1, \ldots, J$.

c) However, when $n > 2$, except for the first of the J cases, there is always a two-node horizonal gap between the $(2J-i)^{th}$ row of CDS1 and the bottom edge of CDS0, where CDS2 with $n > 2$ cannot always be embedded and adjacent. Thus, for $n > 2$, only one case $i = 1$ is effective (e.g., Fig. 5(b) with $n = 3$ and $J = 2$).

APPENDIX B
PROOF OF THE SECOND STEP IN THEOREM 2

b) When $J > 1$ and $i \neq J$, with assistance from Fig. 6(a) and 6(b) but without loss of generality, some vacant areas exist between CDSs along $\boldsymbol{r_1}$ and $\boldsymbol{r_2}$. Considering the cyclic features of the torus, these vacant areas can be filled by all or part regions of several consecutive CDSs placed on the opposite sides. We divide these vacant areas into horizontal e-type and vertical f-type subregions based on the basic CDS shape as shown in Fig. 6(a) and 6(b). Since the positional relationships between adjacent subregions are the same as the CDSs, the successful filling of any e-type subregion and f-type subregion means the remaining subregions can also be filled. Thus, we only need to research the filling methods of arbitrary e-type and f-type subregions.

Horizontally, the vacant subregion on the right beside of CDS0 is selected (e.g., e_1 in Fig. 6(a) and e_0 in Fig. 6(b)). To fill the subregion of bottom edge length $(n-1)$, top edge length $(n+2J-5)$, and height $\Delta\Omega_1$, that is the area containing bottom $\Delta\Omega_1$ rows of one CDS, the left vertex of the last CDS placed along $\boldsymbol{r_2}$ should be on the same vertical column as the rightmost visible node of C0 controller. Thus the last CDS along $\boldsymbol{r_2}$ needs to meet the horizontal difference of $((n-1)+(J-1))$ from CDS0. We know that every time a controller places on $\boldsymbol{r_2}$, the CDS horizontally shifts $\Delta\Theta_2 = g_3\Delta\theta$. Thus $(n+J-2)/g_3$ controllers need to be placed on $\boldsymbol{r_2}$ excluding C0. Further, taking the top row of CDS0 as the top edge, the vertical dimension of the optimal torus lattice M^* is the sum of p_2 vertical offset of CDS along $\boldsymbol{r_2}$ and the upper J rows of the $(p_2+1)^{th}$ CDS, that is (g_4p_2+J).

Vertically, we suppose the $(J+1-i)^{th}$ column from the leftmost vertex of CDS0 is the left edge of the optimal torus lattice. To fill an f-type subregion by the right part of a certain CDS, the rightmost vertex of the satisfactory CDS along $\boldsymbol{r_1}$ needs to be on the same horizontal loop as the rightmost node of a certain f-type subregion which is also always on the same horizontal loop as the i^{th} row of one CDS along $\boldsymbol{r_2}$. Then, we use $\Delta\Omega_1$ and $\Delta\Omega_2$ to respectively characterize the vertical difference between the centerline of the second CDS and the satisfactory CDS along $\boldsymbol{r_1}$ (e.g., $\Delta\Omega$ in Fig. 6(a) and 6(b)), that is $(p_1-1)\,\Delta\Omega_1$ and $i+(p_2'-1)\Delta\Omega_2$. By formula (9) for $\Delta\Omega$, the minimum values of p_1 and p_2' that satisfy $(p_1-1)\,g_2 = i+(p_2'-1)g_4$ are the needful conditions for the optimal SCN construction. Further, to avoid solving the minimum feasible solutions, we find that the right edge of the optimal torus lattice is on the $(J+1-i)^{th}$ column from the rightmost vertex of the satisfactory CDS. So the filled subregion has $(J-i)$ columns, which is equal to the horizontal phase difference between CDS0 and the $(p_2'+1)^{th}$ CDS along $\boldsymbol{r_2}$. Therefore, we have $p_2'\Delta\Theta_2 = J-i$, that is $p_2' = (J-i)/i \in \mathbb{N}^*$. Along $\boldsymbol{r_1}$, the number of columns occupied by the first p_1 CDS in the optimal lattice graph (i.e., yellow box) is g_1p_1, and the number of columns occupied by the $(p_1+1)^{th}$ CDS is $(n+(J-1-g_3p_2')+(i-1))$, so the number of columns of the optimal torus lattice N^* is the sum of the two parts.

REFERENCES

[1] J. Foust, "SpaceX's space-internet woes: Despite technical glitches, the company plans to launch the first of nearly 12,000 satellites in 2019," *IEEE Spectr.*, vol. 56, no. 1, pp. 50–51, Jan. 2019.

[2] I. D. Portillo, B. G. Cameron, and E. F. Crawley, "A technical comparison of three low earth orbit satellite constellation systems to provide global broadband," *Acta Astronautica*, vol. 159, pp. 123–135, Jun. 2019.

[3] I. F. Akyildiz and A. Kak, "The Internet of Space Things/CubeSats," *IEEE Netw.*, vol. 33, no. 5, pp. 212–218, Sep. 2019.

[4] A. Kak and I. F. Akyildiz, "Designing large-scale constellations for the Internet of Space Things with CubeSats," *IEEE Internet Things J.*, vol. 8, no. 3, pp. 1749–1768, Feb. 2021.

[5] W. Saad, M. Bennis, and M. Chen, "A vision of 6G wireless systems: Applications, trends, technologies, and open research problems," *IEEE Netw.*, vol. 34, no. 3, pp. 134–142, May/Jun. 2020.

[6] N. Kato, B. Mao, F. Tang, Y. Kawamoto, and J. Liu, "Ten challenges in advancing machine learning technologies toward 6G," *IEEE Wireless Commun.*, vol. 27, no. 3, pp. 96–103, Jun. 2020.

[7] L. U. Khan, I. Yaqoob, M. Imran, Z. Han, and C. S. Hong, "6G wireless systems: A vision, architectural elements, and future directions," *IEEE Access*, vol. 8, pp. 147029–147044, 2020.

[8] O. Kodheli *et al.*, "Satellite communications in the new space era: A survey and future challenges," *IEEE Commun. Surveys Tuts.*, vol. 23, no. 1, pp. 70–109, 1st Quart., 2021.

[9] J. V. Evans, "Satellite systems for personal communications," *Proc. IEEE*, vol. 86, no. 7, pp. 1325–1341, Jul. 1998.

[10] R. Deng, B. Di, H. Zhang, and L. Song, "Ultra-dense LEO satellite constellation design for global coverage in terrestrial-satellite networks," in *Proc. IEEE Global Commun. Conf. (GLOBECOM)*, Dec. 2020, pp. 1–6.

[11] J. Li, H. Lu, K. Xue, and Y. Zhang, "Temporal netgrid model-based dynamic routing in large-scale small satellite networks," *IEEE Trans. Veh. Technol.*, vol. 68, no. 6, pp. 6009–6021, Jun. 2019.

[12] S. Ji, M. Sheng, D. Zhou, W. Bai, Q. Cao, and J. Li, "Flexible and distributed mobility management for integrated terrestrial-satellite networks: Challenges, architectures, and approaches," *IEEE Netw.*, Jul./Aug. 2021.

[13] R. Deng, B. Di, S. Chen, S. Sun, and L. Song, "Ultra-dense LEO satellite offloading for terrestrial networks: How much to pay the satellite operator?" *IEEE Trans. Wireless Commun.*, vol. 19, no. 10, pp. 6240–6254, Oct. 2020.

[14] R. Deng, B. Di, and L. Song, "How capacity is influenced by ultra-dense LEO topology in multi-terminal satellite systems?" in *Proc. IEEE Wireless Commun. Netw. Conf. (WCNC)*, Seoul, South Korea, May 2020, pp. 1–6.

[15] N. Okati, T. Riihonen, D. Korpi, I. Angervuori, and R. Wichman, "Downlink coverage and rate analysis of low Earth orbit satellite constellations using stochastic geometry," *IEEE Trans. Commun.*, vol. 68, no. 8, pp. 5120–5134, Aug. 2020.

[16] D. Zhou, M. Sheng, X. Wang, C. Xu, R. Liu, and J. Li, "Mission aware contact plan design in resource-limited small satellite networks," *IEEE Trans. Commu.*, vol. 65, no. 6, pp. 2451–2466, Mar. 2017.

[17] M. Sheng, D. Zhou, R. Liu, Y. Wang, and J. Li, "Resource mobility in space information networks: Opportunities, challenges, and approaches," *IEEE Netw.*, vol. 33, no. 1, pp. 128–135, Jan. 2019.

[18] I. del Portillo, B. Cameron, and E. Crawley, "Ground segment architectures for large LEO constellations with feeder links in EHF-bands," in *Proc. IEEE Aerosp. Conf.*, Big Sky, MT, USA, Mar. 2018, pp. 1–14.

[19] S. Xu, X.-W. Wang, and M. Huang, "Software-defined next-generation satellite networks: Architecture, challenges, and solutions," *IEEE Access*, vol. 6, pp. 4027–4041, 2018.

[20] S. Wu, X. Chen, L. Yang, C. Fan, and Y. Zhao, "Dynamic and static controller placement in software-defined satellite networking," *Acta Astronaut.*, vol. 152, pp. 49–58, Nov. 2018.
[21] J. Bao, B. Zhao, W. Yu, Z. Feng, C. Wu, and Z. Gong, "OpenSAN: A software-defined satellite network architecture," in *Proc. ACM Conf. SIGCOMM*, Chicago, IL, USA, Aug. 2014, pp. 347–348.
[22] X. Ding, Z. Zhang, and D. Liu, "Low-delay secure handover for space-air-ground integrated networks," in *Proc. IEEE 31st Annu. Int. Symp. Pers., Indoor Mobile Radio Commun.*, London, U.K., Aug. 2020, pp. 1–6.
[23] K. Xue, W. Meng, H. Zhou, D. S. L. Wei, and M. Guizani, "A light-weight and secure group key based handover authentication protocol for the software-defined space information network," *IEEE Trans. Wireless Commun.*, vol. 19, no. 6, pp. 3673–3684, Jun. 2020.
[24] A. Papa, T. de Cola, P. Vizarreta, M. He, C. Mas-Machuca, and W. Kellerer, "Design and evaluation of reconfigurable SDN LEO constellations," *IEEE Trans. Netw. Service Manage.*, vol. 17, no. 3, pp. 1432–1445, Sep. 2020.
[25] *Solutions for NR to Support Non-Terrestrial Networks (NTN); (Release 16)*, document 3GPP TR 38.821 V16.0.0, Dec. 2019.
[26] H. Tsunoda, U. Dharmaratn, N. Kato, A. Jamalipour, and Y. Nemoto, "SAT04-6: Network controlled handover for improving TCP performance in LEO satellite networks," in *Proc. IEEE Globecom*, San Francisco, CA, USA, Nov. 2006, pp. 1–5.
[27] J. Guo and Y. Du, "Fog service in space information network: Architecture, use case, security and challenges," *IEEE Access*, vol. 8, pp. 11104–11115, 2020.
[28] T. Das and M. Gurusamy, "Controller placement for resilient network state synchronization in multi-controller SDN," *IEEE Commun. Lett.*, vol. 24, no. 6, pp. 1299–1303, Jun. 2020.
[29] *Meet MicroGEO: A Small Comms Satellite for Geostationary Orbit*. Accessed: May 7, 2021. [Online]. Available: https://www.astranis.com/microgeo
[30] *The Software-Defined Future of Satellites*. Accessed: May 7, 2021. [Online]. Available: http://interactive.satellitetoday.com/via/november-2019/the-software-defined-future-of-satellites/
[31] J. Liu, Y. Shi, L. Zhao, Y. Cao, W. Sun, and N. Kato, "Joint placement of controllers and gateways in SDN-enabled 5G-satellite integrated network," *IEEE J. Sel. Area Commun.*, vol. 36, no. 2, pp. 221–232, Feb. 2018.
[32] D. K. Luong, Y.-F. Hu, J.-P. Li, and M. Ali, "Metaheuristic approaches to the joint controller and gateway placement in 5G-satellite SDN networks," in *Proc. IEEE Int. Conf. Commun. (ICC)*, Dublin, Ireland, Jun. 2020, pp. 1–6.
[33] T. Das, V. Sridharan, and M. Gurusamy, "A survey on controller placement in SDN," *IEEE Commun. Surveys Tuts.*, vol. 22, no. 1, pp. 472–503, 1st Quart., 2020.
[34] M. M. Bae, "Resource placement in torus-based networks," *IEEE Trans. Comput.*, vol. 46, no. 10, pp. 1083–1092, Oct. 1997.
[35] P. Krishnan, D. Raz, and Y. Shavitt, "The cache location problem," *IEEE/ACM Trans. Netw.*, vol. 8, no. 5, pp. 568–582, Oct. 2000.
[36] P. Muri, J. McNair, J. Antoon, A. Gordon-Ross, K. Cason, and N. Fitz-Coy, "Topology design and performance analysis for networked earth observing small satellites," in *Proc. Mil. Commun. Conf. (MILCOM)*, Baltimore, MD, USA, Nov. 2011, pp. 1940–1945.
[37] P. G. Buzzi and D. Selva, "Evolutionary formulations for design of heterogeneous Earth observing constellations," in *Proc. IEEE Aerosp. Conf.*, Big Sky, MT, USA, Mar. 2020, pp. 1–10.
[38] *5G; System Architecture for the 5G System (5GS); (Release 16)*, document 3GPP TS 23.501 V16.6.0, Oct. 2020.
[39] *5G; NG-RAN; Architecture Description; (Release 16)*, document 3GPP TS 38.401 V16.3.0, Nov. 2020.
[40] *SpaceX is First With Inter-Satellite Laser Links in Low-Earth Orbit, But Others Will Follow*. Accessed: May 7, 2021. [Online]. Available: https://www.circleid.com/posts/20210127-spacex-first-with-inter-satellite-laser-links-in-low-earth-orbit/
[41] *A New Satellite Architecture for Data*. Accessed: May 7, 2021. [Online]. Available: https://leosat.com/to/solution/
[42] A. U. Chaudhry and H. Yanikomeroglu, "Laser inter-satellite links in a starlink constellation," 2021, *arXiv:2103.00056*. [Online]. Available: http://arxiv.org/abs/2103.00056
[43] A. Carrasco-Casado *et al.*, "Optical communication on CubeSats—Enabling the next era in space science," in *Proc. IEEE Int. Conf. Space Opt. Syst. Appl. (ICSOS)*, Naha, Japan, Nov. 2017, pp. 46–52.
[44] M. Handley, "Delay is not an option: Low latency routing in space," in *Proc. 17th ACM Workshop Hot Topics Netw.*, New York, NY, USA, Nov. 2018, pp. 85–91.
[45] G. Barrenetxea, B. Berefull-Lozano, and M. Vetterli, "Lattice networks: Capacity limits, optimal routing, and queueing behavior," *IEEE/ACM Trans. Netw.*, vol. 14, no. 3, pp. 492–505, Jun. 2006.
[46] A. U. Chaudhry and H. Yanikomeroglu, "Free space optics for next-generation satellite networks," *IEEE Consum. Electron. Mag.*, early access, Oct. 9, 2020, doi: 10.1109/MCE.2020.3029772.
[47] Ö. Korçak and F. Alagöz, "Virtual topology dynamics and handover mechanisms in Earth-fixed LEO satellite systems," *Comput. Netw.*, vol. 53, no. 9, pp. 1497–1511, Jun. 2009.
[48] *O3B—A Different Approach to Ka-Band Satellite System Design and Spectrum Sharing*. Accessed: May 7, 2021. [Online]. Available: https://www.itu.int/dms_pub/itu-r/md/12/iturka.band/c/R12-ITURKA.BAND-C-0010!!PDF-E.pdf
[49] U. Walter, *Astronautics—The Physicals Space Flight*, 3rd ed. Cham, Switzerland: Springer, 2018.
[50] J. Jurski and J. Wozniak, "Routing decisions independent of queuing delays in broadband LEO networks," in *Proc. IEEE Global Telecommun. Conf. (GLOBECOM)*, Honolulu, HI, USA, Nov. 2009, pp. 1–6.

Sijing Ji received the B.E. degree in communication engineering from Zhengzhou University in 2016. He is currently pursuing the Ph.D. degree in communication and information systems with the School of Telecommunications Engineering, Xidian University, China. His research interests include architectures, protocols, and mobility management in satellite-terrestrial integrated networks.

Di Zhou (Member, IEEE) received the B.E. and Ph.D. degrees in communication and information systems from Xidian University, Xi'an, China, in 2013 and 2019, respectively. She was a Visiting Ph.D. Student with the Department of Electrical and Computer Engineering, University of Houston, from 2017 to 2018. Since 2019, she has been with the Broadband Wireless Communications Laboratory, School of Telecommunications Engineering, Xidian University, where she currently holds a faculty postdoctoral position. Her research interests include routing, dynamic resource allocation, and mission planning in space-terrestrial integration networks.

Min Sheng (Senior Member, IEEE) joined Xidian University in 2000, where she is currently a Full Professor and the Director of the State Key Laboratory of Integrated Services Networks. She is the Vice Chair of IEEE Xi'an Section. She has published over 200 refereed papers in international leading journals and key conferences in the area of wireless communications and networking. Her current research interests include space-terrestrial integration networks, intelligent wireless networks, and mobile *ad hoc* networks. She received China National Funds for Distinguished Young Scientists in 2018. She is an Editor for IEEE COMMUNICATIONS LETTERS and IEEE TRANSACTION ON WIRELESS COMMUNICATIONS.

Jiandong Li (Fellow, IEEE) received the B.E., M.S., and Ph.D. degrees in communications engineering from Xidian University, Xi'an, China, in 1982, 1985, and 1991, respectively. He has been a Faculty Member with the School of Telecommunications Engineering, Xidian University, since 1985, where he is currently a Professor and the Vice Director of the Academic Committee, State Key Laboratory of Integrated Service Networks. He was a Visiting Professor with the Department of Electrical and Computer Engineering, Cornell University, from 2002 to 2003. He was awarded as a Distinguished Young Researcher from NSFC and a Changjiang Scholar from the Ministry of Education, China. His major research interests include wireless communication theory, cognitive radio, and signal processing. He served as the General Vice Chair for CHINACOM 2009 and the TPC Chair of IEEE ICCC 2013.